DNA interaction with Ru(II) and Ru(II)/Cu(II) complexes containing azamacrocycle and dppz residues. A thermodynamic, kinetic and theoretical study

ARTICLE *in* DALTON TRANSACTIONS · NOVEMBER 2010

Impact Factor: 4.2 · DOI: 10.1039/c0dt00552e · Source: PubMed

DNA interaction with Ru(II) and Ru(II)/Cu(II) complexes containing azamacrocycle and dppz residues. A thermodynamic, kinetic and theoretical study.†

Carla Bazzicalupi,[a] Silvia Biagini,[a] Antonio Bianchi,*[a] Tarita Biver,*[b] Alessia Boggioni,[b] Claudia Giorgi,[a] Paola Gratteri,[c] Marino Malavolti,[a] Fernando Secco,[b] Barbara Valtancoli[a] and Marcella Venturini[b]

Received 26th May 2010, Accepted 22nd July 2010
DOI: 10.1039/c0dt00552e

Ru(II) complexes that bring together the properties of the dppz (dipyrido[3,2-a:2′,3′-c]phenazine) intercalating residue and the properties of metal-coordinating macrocycles (L = 4,4′-(2,5,8,11,14-pentaaza[15])-2,2′-bipyridilophane) have been synthesised and their protonation and affinity for copper(II) was analysed. Ru(bpy)(dppz)L^{2+} ($D2^{2+}$) and Ru(dppz)$_2L^{2+}$ ($D3^{2+}$) were found to interact with DNA but the binding mode is not simple and its features strongly depend both on the ligand structure and on the [DNA]/[complex] ratio. Equilibrium measurements (spectrophotometric and spectrofluorometric titrations), kinetics (stopped-flow technique) and theoretical calculations all concur in suggesting that for the less hindered $D2^{2+}$ an important contribution of external binding, driven by dye–dye interactions, is operative, as revealed by the onset of positive cooperativity. On the contrary, for the bulkier $D3^{2+}$ complex dye–dye interactions are less effective, resulting in an intercalation process with lower dppz penetration within DNA slots. The Ru(bipy)$_2L^{2+}$($D1^{2+}$)/DNA system was also analysed for comparison and helped in showing the non negligible contribution of the macrocycle to the binding process. The binding affinities of the macrocycle copper complexes for DNA are lower than those of their copper-free analogues only in the case of $D1^{2+}$, whereas an affinity enhancement in agreement with the charge increase upon copper coordination is observed for $D2^{2+}$ and $D3^{2+}$. Copper coordination produces complete loss of the cooperative behaviour in the case of $D2^{2+}$. Further mechanistic details are discussed.

1. Introduction

In the last few years transition metal complexes bearing functionalities able to intercalate into nucleic acids have attracted considerable interest due to their potential applications as DNA and RNA sequence probes or anticancer drugs.[1–3] In particular, ruthenium complexes are the subject of great attention in the field of medicinal chemistry as antitumour agents with selective antimetastatic properties and low systemic toxicity, that penetrate reasonably well into tumour cells and effectively bind to DNA.[4,5] In this context, Ru(II) complexes containing dipyrido[3,2-a:2′,3′-c]phenazine (dppz) ligands have focused much research mainly because this group shows efficient intercalation properties and, upon intercalation, the Ru(II) complexes may behave as sequence sensitive DNA light-switches; consequently they have been used as luminescent probes for DNA diagnostics.[6–11] The MLCT excited state of these complexes is characterized by a long-lived luminescence associated to a state in which the promoted electron is localized on the dppz ligand.[12–14] Nevertheless, their emission, is extremely weak in water, likely due to proton transfer to the phenazine nitrogen atoms of the photoexcited complex.[14–17] However, the luminescence of these complexes revives when interacting with DNA, as water molecules surrounding dppz groups are released upon intercalation, giving rise to the light-switching effect. Although intercalation of dppz ligand is generally accepted as a fundamental element of the interaction of metal complexes bearing this residue with DNA, the mode of interaction is still a subject of debate. In fact, different interaction modes appear to be possible, including the "side-on" and the "head-on" intercalation observed for the DNA/[Os(phen)$_2$(dppz)]$^{2+}$ (phen = phenanthroline) system[18] and the adducts of different stoichiometry formed by [Ru(phen)$_2$(dppz)]$^{2+}$ featuring "surface" or partial intercalative interaction.[19,20]

In recent years we have studied the interaction with DNA of Zn(II) and Cu(II) metallo-intercalators based on polyaza-macrocyclic ligands containing a phenanthroline group in their cyclic skeleton;[21,22] these complexes display a preliminary fast interaction with DNA to form externally bound forms which are successively converted into internally bound complexes by intercalation. Stronger interaction with DNA[21] and an active role in DNA cleavage[22] was observed for the Cu(II) complexes.

On this basis, we thought to bring together the properties of Ru(II) complexes containing the dppz ligand and the properties of macrocyclic metallo-intercalators. To this purpose we have synthesized the metal complexes $D2^{2+}$ and $D3^{2+}$ shown in Fig. 1, which are ideally derived from $D1^{2+}$ *via* substitution of bipyridine (bpy) with dppz groups. In $D2^{2+}$ the only intercalating residue is

[a]*Dipartimento di Chimica "Ugo Schiff", Università di Firenze, Via della Lastruccia 3, 50019, Sesto Fiorentino, Italy. E-mail: antonio.bianchi@unifi.it; Fax: +39-055 4573364*
[b]*Dipartimento di Chimica e Chimica Industriale, Università di Pisa, Via Risorgimento 35, 56126, Pisa, Italy. E-mail: tarita@dcci.unipi.it; Fax: 39-050-2219260*
[c]*Dipartimento di Scienze Farmaceutiche, Università di Firenze, Via Ugo Schiff 6, 50019, Sesto Fiorentino, Italy*
† Electronic supplementary information (ESI) available: Experimental details. See DOI: 10.1039/c0dt00552e

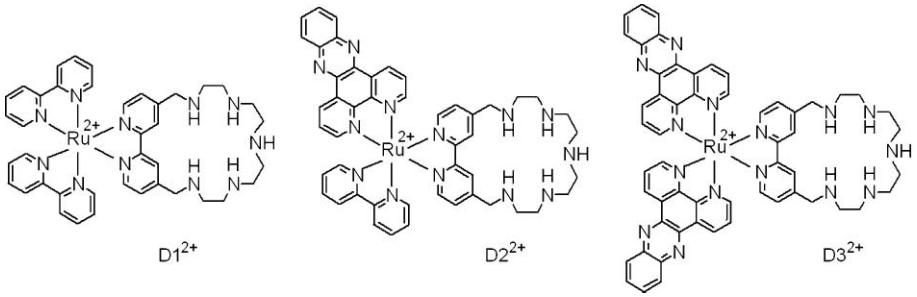

Fig. 1 The Ru(II) complexes containing bpy, dppz and 4,4′-(2,5,8,11,14-pentaaza[15])-2,2′ bipyridilophane (L) ligands.

supposed to be dppz, whereas in D3^{2+} two dppz are present, to yield on one hand a more hindered molecule, on the other hand a species with higher intercalating opportunities.

These complexes contain a macrocyclic bipyridilophane polyamine (L), bearing two separated binding units (the macrocyclic cavity constituted by five aliphatic amine groups and the external chelating bpy unit), which is able to bind metal ions both inside and outside the cavity.[23–27] We have shown that the polyprotonated species as well as the Zn(II) complexes formed by L act as multifunctional receptors toward substrate species, like ATP, involving electrostatic, H-bond, coordinative, and π-stacking interactions in the formation of the substrate-receptor adducts.[27] Furthermore, the D1^{2+} complex containing protonated amine groups in the macrocyclic ring can act as a photocatalyst in oxidation/reduction processes involving anionic species.[28] These are the reasons why L was the ligand of choice to prepare the D2^{2+} and D3^{2+} complexes for DNA binding studies.

In this paper we describe the synthesis of D2^{2+} and D3^{2+}, their metal binding properties toward Cu(II) and the characteristics of the interaction of DNA with D1^{2+}, D2^{2+} and D3^{2+} and their Cu(II) complexes.

2. Experimental

2.1. Materials

All chemicals employed for the synthesis of the D1^{2+}, D2^{2+} and D3^{2+} complexes (Fig. 1) and for all subsequent studies were reagent grade and used without further purification. The complex D1^{2+},[28] the macrocycle 4,4′-(2,5,8,11,14-pentaaza[15])-2,2′-bipyridilophane (L),[23] the dipyrido[3,2-a:2′,3′-c]phenazine (dppz),[29] the polymer $[Ru(CO)_2Cl_2]_n$, $[Ru(bpy)(CO)_2Cl_2]$ and $[Ru(bpy)(CO)Cl_2]_2$ [30] were prepared *via* literature methods.

2.1.1. Synthesis of D3^{2+}. The synthetic procedure adopted to prepare D3^{2+} is schematized in Fig. 2.

*Preparation of RuL(CO)$_2$Cl$_2$ (**2**).* A solution of the polymer **1** (54.9 mg, corresponding to 0.20 mmol of Ru) and L·5HBr (170 mg, 0.18 mmol) in 3.5 cm^3 of methanol was refluxed for 3 h in a nitrogen atmosphere. The resulting solution was then evaporated under reduced pressure and the solid residue was suspended in ethanol (20 cm^3) to separate the insoluble polymer **1** from the soluble compound **2**. The suspension was filtered, then the solvent was removed by evaporation under reduced pressure and the solid obtained was dried in vacuum at 40 °C to give **2** in the form of **2**·5HBr·11H$_2$O. Yield: 182 mg (84%). ^{1}H NMR (400 MHz, D$_2$O pH = 2) δ = 9.35 (d, 2H), 9.01 (s, 2H), 7.89 (d, 2H), 4.73 (s, 4H), 3.76 (m, 8H), 3.63 (m, 8H). Anal. Calc. for $C_{22}H_{58}Br_5Cl_2N_7O_{13}Ru$: C, 22.02; H, 4.87; N, 8.17; found: C, 22.1; H, 4.8; N, 8.2%.

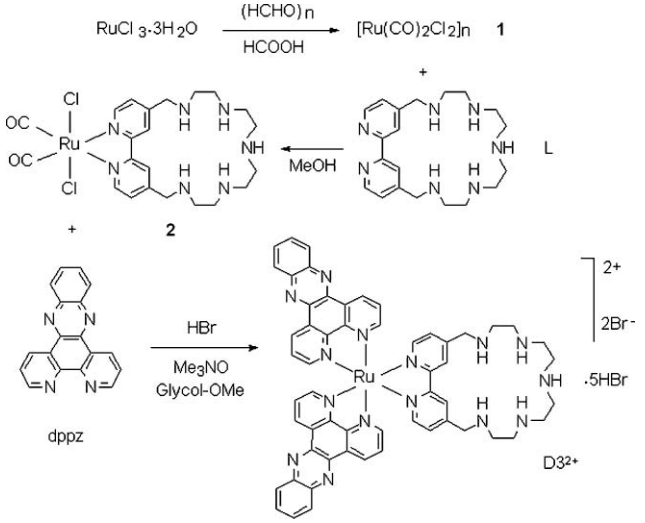

Fig. 2 Reaction sequence for the synthesis of D3^{2+}.

Preparation of D3Br$_2$·5HBr·10.4H$_2$O. A 10 cm^3 of 2-methoxyethanol were degassed under reflux for 20 min while nitrogen was bubbled into the boiling solvent. The nitrogen atmosphere was then maintained and dppz (118 mg, 0.41 mmol), **2** (176 mg, 0.15 mmol) and trimethylamine N-oxide (98.1 mg, 0.88 mmol) were added. The resulting solution was boiled for 3 h during which the colour turned from pale orange to deep red. The solution was evaporated to dryness under reduced pressure, the residue was washed thoroughly with acetone, dissolved in the minimum amount of water, acidified with HBr (pH 2) and precipitated by slow addition of acetone. The compound was dried in vacuum at room temperature. Yield: 131 mg (47%). ^{1}H NMR (400 MHz, D$_2$O pH = 2) δ = 8.8 (d, 4H), 8.6 (d, 2H), 8.53 (s, 2H), 8.07 (dd, 4H), 8.0 (d, 4H), 7.67 (dd, 4H), 7.3 (t, 4H), 7.15 (d, 2H), 4.6 (m, 4H), 3.5 (m, 16H). ^{13}C NMR (400 MHz, D$_2$O pH = 2) δ = 157.6, 153.1, 150.0, 149.6, 141.6, 138.7, 133.8, 129.8, 128.0, 127.4, 125.7, 49.5, 46.6, 45.0, 44.0. ESI-MS: m/z = 1035.00 ($[C_{57}H_{51}N_{15}Ru]^+$), 517.00 ($[C_{57}H_{51}N_{15}Ru]^{2+}$). UV-Vis ($\lambda$/nm, ε/M^{-1}cm^{-1}) (H$_2$O, pH 2.0): 276 (111 891), 360 (33 215), 450 (19 106); (H$_2$O, pH 11.0): 276 (95 610), 360 (26 382), 450 (15 635). Anal. Calc. for $C_{56}H_{81.8}Br_7N_{15}O_{10.4}Ru$: C, 37.64; H, 4.33; N, 11.76; found: C, 37.8; H, 4.3; N, 11.7%.

2.1.2. Synthesis of D2^{2+}. The synthetic procedure adopted to prepare D2^{2+} is schematized in Fig. 3.

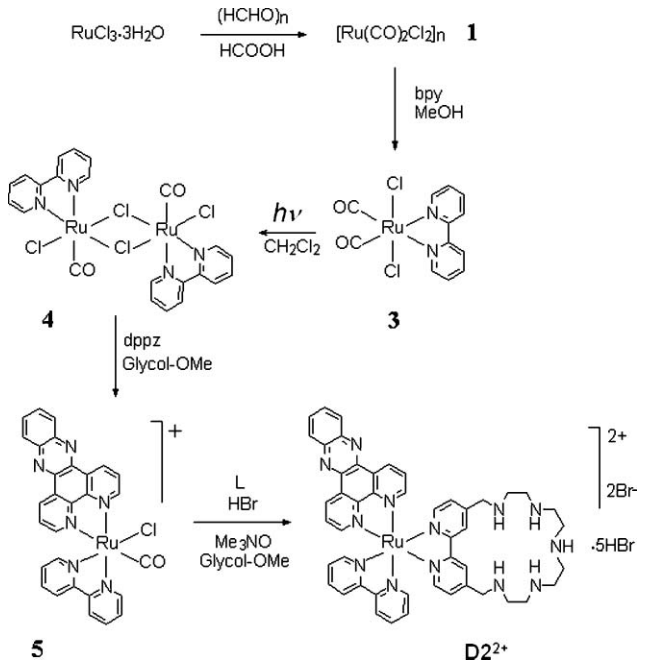

Fig. 3 Reaction sequence for the synthesis of $D2^{2+}$.

Synthesis of [Ru(bpy)(dppz)(CO)Cl]Cl·3.6H$_2$O (5). 10 cm^3 of 2-methoxyethanol were degassed under reflux for 20 min while nitrogen was bubbled into the boiling solvent. The nitrogen atmosphere was then maintained and compound **4** (104 mg, 0.14 mmol) was added. The resulting suspension was boiled for 30 min after which dppz (108 mg, 0.37 mmol) was added. The reflux was maintained for 2 h in the darkness. The slow formation of complex **5** is manifested by transformation of the orange suspension into a yellow–orange solution. The solvent was removed by evaporation under reduced pressure and the resulting solid compound was dried in vacuum at 40 °C. The solid was then suspended in 20 cm^3 of water and the mixture was sonicated for 10 min, cooled to 4 °C and filtered to remove the solid residue. The solution was successively evaporated to dryness and the resulting solid compound was dried in vacuum at 40 °C. Yield: 53 mg (54%). ^{1}H NMR (400 MHz, DMSO-d$_6$) δ = 9.83 (t, 2H), 9.74 (d, 1H), 9.56 (d, 1H), 8.94 (d, 1H), 8.76 (d, 1H), 8.52 (m, 3H), 8.36 (m, 1H), 8.18 (m, 2H), 8.07 (m, 4H), 7.79 (d, 1H), 7.34 (t, 1H). ^{13}C NMR (400 MHz, DMSO-d$_6$) δ = 206.8, 158.0, 157.3, 153.1, 142.7, 140.8, 139.9, 136.3, 135.1, 133.1, 130.0, 128.7, 128.5, 128.0, 125.3, 124.9. UV-Vis (λ/nm, ε/M^{-1} cm^{-1}) (H$_2$O): 276 (68 960), 360 (15 300). UV-Vis (λ/nm, ε/M^{-1}cm^{-1}) (H$_2$O): 276 (68 960), 360 (15 300). Anal. Calc. for $C_{29}H_{25.2}Cl_2N_6O_{4.6}Ru$: C, 49.52; H, 3.61; N, 11.95; found: C, 49.9; H, 3.3; N, 11.9%.

Synthesis of D2Br$_2$·5HBr·5H$_2$O. 10 cm^3 of 2-methoxyethanol were degassed under reflux for 20 min while nitrogen was bubbled into the boiling solvent. The nitrogen atmosphere was then maintained and the macrocycle L (97.4 mg, 0.11 mmol), compound **5** (86.1 mg, 0.12 mmol), and trimethylamine N-oxide (36.5 mg, 0.33 mmol) were added. The resulting mixture was boiled for 3 h in the dark while its colour turned from pale orange to deep red. The solvent was then removed under reduced pressure and the crude solid was washed several times with acetone to remove the unreacted **5** compound. The solid residue was successively dried in vacuum at 40 °C and recrystallized from the minimum amount of aqueous HBr upon addition of acetone. Yield: 37 mg (22%). ^{1}H NMR (400 MHz, D$_2$O pH = 2) δ = 8.8 (d, 2H), 8.65 (m, 4H), 8.25 (m, 4H), 8.10 (d, 2H), 8.0 (d, 2H), 7.80 (m, 4H), 7.50 (dd, 2H), 7.20 (d, 2H), 7.10 (dd, 2H), 4.6 (m, 4H), 3.5 (m, 16H). ^{13}C NMR (400 MHz, D$_2$O pH = 2) δ = 157.7, 157.0, 153.6, 152.0, 150.3, 142.4, 141.3, 140.2, 133.8, 130.4, 128.9, 128.0, 127.3, 125.0, 124.3, 49.5, 47.0, 45.3, 44.2. ESI-MS: m/z = 454.66 ([$C_{48}H_{49}N_{13}Ru$]$^{2+}$), 303.44 ([$C_{48}H_{49}N_{13}Ru$]$^{3+}$). UV-Vis (λ/nm, ε/M^{-1} cm^{-1}) (H$_2$O, pH 2.0): 283 (130 400), 360 (26 500), 450 (18 195); (H$_2$O, pH 11.0): 283 (120 391), 360 (22 599), 450 (18 195). Anal. Calc. for $C_{48}H_{64}Br_7N_{13}O_5Ru$: C, 36.87; H, 4.12; N, 11.64; found: C, 37.5; H, 4.26; N, 11.70%.

Table 1 Protonation and Cu(II) complexation constants of $D3^{2+}$ determined in 0.10 M NMe_4Cl solutions at 25 ± 0.1 °C

	log K
$D3^{2+} + H^+ = D3H^{3+}$	8.52(9)[a]
$D3H^{3+} + H^+ = D3H_2^{4+}$	5.9(1)
$D3H_2^{4+} + H^+ = D3H_3^{5+}$	4.4(1)
$D3H_3^{5+} + H^+ = D3H_4^{6+}$	2.6(1)
$D3H_4^{6+} + H^+ = D3H_5^{7+}$	2.7(1)
$D3^{2+} + Cu^{2+} = [CuD3]^{4+}$	8.82(4)
$[CuD3]^{4+} + H^+ = [CuD3H]^{5+}$	6.36(3)
$[CuD3H]^{5+} + H^+ = [CuD3H_2]6^+$	4.49(1)
$[CuD3H_2]^{6+} + H^+ = [CuD3H_3]^{7+}$	2.89(2)
$[CuD3]^{4+} + OH^- = [CuD3(OH)]^{3+}$	4.82(7)
$[CuD3OH]^{3+} + OH^- = [CuD3(OH)_2]^{2+}$	3.86(6)

[a] Values in parentheses are standard deviations on the last significant figures.

The solutions of the ruthenium complexes were prepared by dissolving weighed amounts of the solid into doubly distilled water and kept in the dark at 4 °C; their concentrations are expressed in molarity and indicated as C_D. Calf thymus DNA (CT-DNA) was purchased from Sigma as the lyophilised sodium salt. It was dissolved in water and sonicated as described below. Stock solutions of the polynucleotide were standardised spectrophotometrically, using ε = 13200 M^{-1} cm^{-1} at 260 nm as obtained from the sample certificate for polynucleotides concentrations expressed in molarity of base-pairs (indicated as C_P). Within the study of ruthenium complexes interaction with DNA, all solutions were buffered at pH = 7.0 by 0.01 M or 3 × 10^{-3} M NaCac (sodium cacodylate (CH_3)$_2$AsO$_2$Na), while the ionic strength was adjusted by suitable additions of sodium chloride. Note that at pH = 7.0 the ruthenium complexes used are respectively in the forms H_2D1^{4+} and $CuD1^{4+}$,[28] $HD3^{3+}$ and $CuD3^{4+}$ (Table 1). Unfortunately, it was not possible to carry out a potentiometric study of the protonation and complexation equilibria of $D2^{2+}$ due to its too low solubility in the pH range above 5; nevertheless, on the basis of the results obtained for $D1^{2+}$ and $D3^{2+}$, it will be assumed that at pH = 7.0 the copper complex is in the $CuD2^{4+}$ form, whereas in the absence of copper both H_2D2^{4+} and $HD2^{3+}$ forms are simultaneously present (the $HD2^{3+}$ notation will be used in the text for simplicity).

Doubly-distilled water from a Millipore Milli-Q water purification system was used to prepare the solutions and as the reaction medium.

2.2. Methods

2.2.1. Potentiometric measurements. All pH-metric measurements (pH = –log [H^+]) employed for the determination of equilibrium constants were carried out in 0.10 M NMe_4Cl solutions at 25.0 ± 0.1 °C, by using the equipment and the methodology that has been already described.[31] The combined Hamilton electrode (LIQ-GLASS 238000/08) was calibrated as a hydrogen concentration probe by titrating known amounts of HCl with CO_2-free NaOH solutions and determining the equivalent point by Gran's method[32] which allows one to determine the standard potential $E°$ and the ionic product of water (pK_w = 13.83(1) at 25.0 ± 0.1 °C in 0.10 M NMe_4Cl). At least three measurements were performed for each system in the pH ranges 2.5–10.5. In all experiments the total dye concentration, C_D, was about 5×10^{-4} M. In the metal complexation experiments the metal cation concentration was about [cation] = $0.8C_D$. The computer program HYPERQUAD[33] was used to calculate the equilibrium constants from e.m.f. data.

2.2.2. ^{1}H and ^{13}C NMR measurements. ^{1}H and ^{13}C NMR spectra were recorded at 25 °C on a Bruker Advance III 400 MHz instrument. In ^{1}H NMR spectra peak positions are reported relative to HOD at δ 4.79 ppm (D_2O), while in ^{13}C spectra peak positions are reported relative to 1,4-dioxane at δ 67.2 ppm (D_2O). The pD of sample solutions was adjusted by small amounts of 0.01 M NMe_4OD or DCl. The pH was calculated from the measured pD value by using the relationship pH = pD – 0.40.[34]

2.2.3. DNA sonication. DNA sonication was carried out using a MSE-Sonyprep sonicator, by applying to suitable DNA samples (10 mL of CT-DNA *ca.* 2×10^{-3} M) seven repeated cycles of 10 s sonication and 20 s pause, at an amplitude of 14 microns. The sonicator tip was introduced directly into the solution, this being kept in an ice bath to minimize thermal effects due to sonication. Agarose gel electrophoresis tests indicated that the polymer length was reduced to *ca.* 800 base pairs.

2.2.4. Spectral measurements. Absorption spectra were recorded on a Perkin–Elmer Lambda 35 spectrophotometer and fluorescence emission spectra on a Perkin–Elmer LS 55 spectrofluorometer. Both spectrophotometer and spectrofluorometer are equipped with jacketed cell holders, with temperature control within ± 0.1 °C. The DNA titrations were carried out at 25.0 ± 0.1 °C by adding increasing amounts of the polynucleotide directly into the cell containing the dye solution. In the particular case of the absorbance titrations for the DNA/H_2D1^{4+} system in the UV range, the experiments were carried out in the difference mode, *i.e.* exactly equivalent amounts of DNA were added into both reference and sample cells of the spectrophotometer. Experimental data were analysed by means of non-linear least-square fitting procedures performed by a JANDEL (AISN software) program.

2.2.5. Electrophoresis experiments. The electrophoresis experiments were carried out on the DNA/$HD2^{3+}$, DNA/$CuD2^{4+}$, DNA/$HD3^{3+}$ and DNA/$CuD3^{4+}$ systems, alone or in the presence of H_2O_2 (1.8×10^{-3} M), using a LKB 2050 Midget Electrophoresis Unit with Tris-acetate-EDTA as a buffer (pH = 7.4) and agarose gels (1% in weight) stained with 1 μM ethidium bromide. The DNA concentration is kept constant in all experiments (2.5×10^{-4} M); for $CuD2^{4+}$ complex formation is achieved by 5 : 1 copper addition to $D2^{2+}$, whereas for $CuD3^{4+}$ a 1 : 1 ratio was sufficient to ensure quantitative copper complex formation. The experiments were performed 48 h after reagents mixing and took *ca.* $\frac{1}{2}$h at 65 V and 50 mA.

2.2.6. Kinetic experiments. The kinetic study on the $D2^{2+}$ and $D3^{2+}$ complexes interaction with DNA was done by means of the stopped-flow technique with absorbance detection (λ = 360 nm) at 25 °C, pH = 7.0, I = 0.10 M (0.09 M NaCl and 0.01 M NaCac). The stopped-flow apparatus, constructed in our laboratory, uses a Hi-Tech (TgK Scientific, Bradford on Avon, UK) KinetAsyst SHU-61SX2 mixing unit connected to a spectrophotometric line by two optical guides. The acquired signal is transferred to a personal computer, where it is analysed by means of non-linear least-square fitting procedures performed by a JANDEL (AISN software) program. Experiments were done by varying the ruthenium complex concentration, C_D, (from 6.6×10^{-6} to 9.4×10^{-6} M for the DNA/$HD2^{3+}$ system, from 2.1×10^{-6} to 1.0×10^{-5} M for the DNA/$HD3^{3+}$ system) and the DNA concentration, C_P (from 4.0×10^{-5} to 2.2×10^{-4} for the DNA/$HD2^{3+}$ system, from 2.0×10^{-5} to 2.0×10^{-4} M for the DNA/$HD3^{3+}$ system), but always under pseudo first-order conditions ($C_P/C_D > 6$ for the DNA/$HD2^{3+}$ system, $C_P/C_D > 8$ for the DNA/$HD3^{3+}$ system). Each experiment was repeated at least ten times, and the observed spread of time constants was found to be within 10%. Average values of the measured time constants are used for the analysis of the kinetic experiments.

2.2.7. Molecular modelling. All computations were performed on a dual core AMD Opteron and 4 processors running Linux. Starting conformations for both metal complexes and DNA were built using the Builder module in Maestro v.7.5.[35] The metallic core of both Δ and Λ configurations of $HD2^{3+}$, H_2D2^{4+}, $HD3^{3+}$ and H_2D3^{4+} ruthenium complexes were built by using the crystallographic coordinates from CCDC refcodes DAXXIJ and DAXZIL.[36] Partial charges were estimated by fitting of the electrostatic potential (Jaguar software,[37] DFT/B3LYP[38] level of theory with the LACVP**+ basis set[39]). A total of five B-type double helix DNA decamers, featuring 60% CG and 40% AT base-pair composition similarly to CT-DNA (ATATATATAT, GCGCGCGCGC, ATCGCGCGAT, CGCGATATCG, CGATCGATCG), and two dodecamers (GCGCGCGCGCGC, ATATATATATAT) were used. Intercalation sites of CG and/or AT types were conveniently built in the centre of the polymers for each DNA sequence. In order to locate the first complex molecule, docking calculations were performed using the Glide program[40] for the Δ and Λ configurations of the four studied cations and all the 10-mer DNA sequences. Default input parameters were used in all computations (no scaling factor for the vdW radii of non polar DNA atoms, 0.8 scaling factor for non polar ligand atoms). The grids for the docking (32 Å edges for the enclosing box) were centred on the centroid of the appropriate residues, chosen according to the intercalative and non-intercalative binding modes. Upon completion of each docking calculation, three poses per ligand were saved and ranked according to the glide-score. Once the preferred orientations for the metal complex-DNA adducts were recognized, a second series of docking procedures was carried out in order to investigate the presence of dye–dye interactions that might be responsible for cooperative behaviours.

In this case, the grids for the docking (32 Å edges for the enclosing box) were prepared on the GCGCGCGCGCGC/D2, GCGCGCGCGCGC/D3, and ATATATATATAT/D3 adducts centred on the centroid of the appropriate residues, chosen as near as possible to the metal complexes, according to the intercalative and non-intercalative binding modes. A maximum of three poses for each chiral configuration of the metal complexes were saved, minimized with Impact,[41] by using the OPLS2005 force-field-based conjugate gradient minimization routine (atomic charges from file, maximum number of minimization cycles 100, energy change criterion 0.05 kcal mol^{-1} $Å^{-1}$, gradient criterion 0.01, ruthenium and bipyridine nitrogen atoms frozen, GB/SA continuum representation of the solvent[41]) and their energy were evaluated by single-point QM/MM calculations performed by means of the Qsite software[42] (QM region constituted by the two metal complex units and treated at DFT/B3LYP[38] level of theory with the LACVP basis set,[39] MM region constituted by the DNA polymer and treated with Impact,[41] OPLS2005 force-field). Continuum representation of the solvent was used by means of the Poisson–Boltzmann solver equation.[43]

3. Results

3.1. Synthesis

According to the literature,[28] the synthesis of $D1^{2+}$ was carried out by reaction of $Ru(bpy)_2Cl_2$ with the macrocyclic ligand L. The same procedure was attempted for the preparation of $D3^{2+}$, but the intermediate compound $Ru(dppz)_2Cl_2$, which was prepared by the method reported for $Ru(bpy)_2Cl_2$,[44] displayed a very poor solubility in organic solvents and in water, thus preventing the successive reaction with L. For this reason a different synthetic path (Fig. 2) based on the $[Ru(CO)_2Cl_2]_n$ polymer (**1**) was followed to obtain $D3^{2+}$. This polymer can be obtained by reaction of $RuCl_3 \cdot 3H_2O$ with formic acid and paraformaldehyde in dimethylformamide.[45] Reaction of the polymer with L to give $RuL(CO)_2Cl_2$ (**2**) was performed by adapting a literature procedure.[46] An excess of the polymer **1** was used to favour the formation of **2**, taking into account that the unreacted product can be easily removed by washing the crude mixture with ethanol. Preparation of **2** by the last reaction can be achieved in a reasonable yield (47%) only when L is used as its hydrobromic salt L·6HBr, while the same reaction performed in the presence of the free ligand did not furnish the desired compound. Most likely protonation of the aliphatic amine groups in the hydrobromic salt protects this groups from the possible reaction with Ru(II), thus favouring metal binding to the unprotonated nitrogen atoms of the bpy moiety. The reaction of **2** with dppz was then performed in the presence of Me_3NO working as a decarbonylation reagent.[45]

A similar procedure based on the use of the $[Ru(CO)_2Cl_2]_n$ polymer (**1**) was adopted to prepare $D2^{2+}$ (Fig. 3). In this case, the polymer was used to insert bpy as the first ligand, affording $Ru(bpy)(CO)_2Cl_2$ (**3**) which was converted into the dimer $[Ru(bpy)(CO)Cl_2]_2$ (**4**) by light irradiation of a CH_2Cl_2 solution and successive removal of the solvent.[30] By treating the dimer **4** with dppz in boiling 2-methoxyethanol, the compound **5** can be obtained in fairly good yield (54%). An excess of dppz was used to favour the formation of this compound, since the unreacted dppz can be easily removed by extraction of **5** with water. The successive addition of the macrocyclic ligand L requires the action of the decarbonylation reagent Me_3NO. We also explored the alternative procedure of adding L to the dimer **4**, but the yield of the reaction was very poor. It is to be noted that the formation of dimeric compounds like **4** can take place upon UV-Vis light irradiation of different $Ru(pp)(CO)_2Cl_2$ complexes containing bidentate ligands (pp).[47] A similar reaction is also possible when solutions of compound **2** are handled in the presence of light during the synthesis of $D3^{2+}$ (Fig. 2). Nevertheless, the possible formation of a dimer from **2** does not affect the course of the reaction with dppz to give $D3^{2+}$.

Characterisation of $D2^{2+}$ and $D3^{3+}$ was performed by means of elemental analysis, ESI-MS, UV-vis, and ^1H and ^{13}C NMR spectra. Examples of ^1H NMR spectra are reported in Fig. S1 and S2.† Signal assignment was performed on the basis of the individual spectra of L, bipy, and dppz molecules as well as on the basis of the spectra previously reported[28] for $D1^{2+}$. In the case of $D1^{2+}$, the crystal structure of its triprotonated form confirmed that the arrangement of ligands around the Ru(II) ion was as expected on the basis of the synthetic procedure adopted and the solution information furnished by NMR spectra.[28]

3.2. Protonation and Cu(II) complexation

Protonation and Cu(II) complexation constants of $D3^{2+}$ determined by potentiometric measurements in 0.10 M NMe_4Cl solutions at 25 ± 0.1 °C are shown in Table 1.

As shown by the distribution diagram of the protonated species (Fig. 4), $D3^{2+}$ starts binding protons below pH 10 with the formation of the monoprotonated $HD3^{3+}$ form which becomes the main species at physiological pH where it is formed in more than 90%. Successive stepwise protonation takes place in more acidic solutions according to the pattern expected for polyamine macrocycles.[48] In particular, the first three protons can bind amine groups separated by $CH_2CH_2NHCH_2CH_2$ chains, giving rise to moderate electrostatic repulsion. On the contrary, the last two H^+ ions are necessarily located between charged (protonated) nitrogen atoms with increasing repulsion. Accordingly, the last two protonation processes, occurring on amine groups with similar environments, take place with small protonation constants which are of the same value within experimental errors (Table 1).

Cu(II) complexation by the macrocyclic component (L) of $D3^{2+}$ takes place over the whole pH range investigated (2.5–10.5) (Fig. S3 of the ESI†). $CuD3^{4+}$ is the main species at physiological pH, being formed in about 90%. This species gives rise to mono-, di- and tri-protonated complexes on lowering the solution pH, while deprotonation of metal-coordinated water molecules occurs in alkaline solution leading to the formation of mono- and di-hydroxo complexes. In particular, the equilibrium constant for the protonation of $CuD3^{4+}$ to form $CuD3H^{5+}$ (log K = 6.39, Table 1) is within the range of the first two protonation constants of the Cu(II)-free ligand (log K = 8.52–5.9, Table 1), suggesting that protonation of the complex occurs on a nitrogen atom not involved in Cu(II) binding. Accordingly, at most four amine groups of the macrocycle are expected to participate in the coordination to Cu(II), in agreement with the metal ion coordination environment previously observed in the crystal structure[25] of a Cd(II) complex with L. This means that the macrocyclic ligand L is not able to fulfil the coordination sphere of Cu(II) favouring the binding of

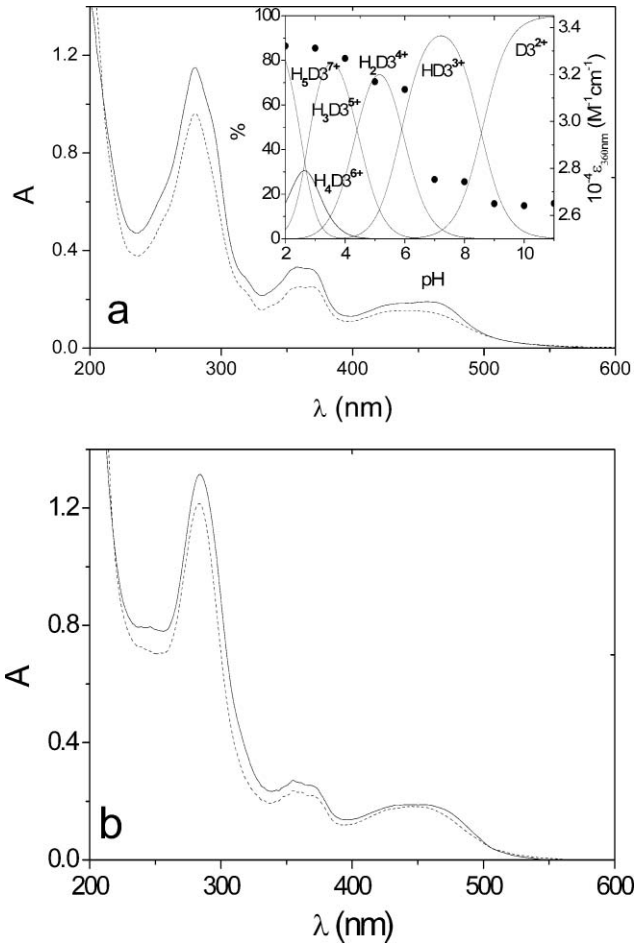

Fig. 4 Absorption spectra of $D3^{2+}$ (a) and $D2^{2+}$ (b) recorded in water at pH 2 (—) and pH 11 (···). $[D3^{2+}] = [D2^{2+}] = 1 \times 10^{-5}$ M, T = 25 °C. Inset: Distribution diagram of the protonated species of $D3^{2+}$ and related absorption coefficients at 360 nm (black circles) as a function of pH.

exogenous species. This is a promising feature of $D3^{2+}$, since the coordinated Cu(II) ion might play an active role in DNA binding.

As already noted in the experimental section, it was not possible to determine the protonation and complexation equilibria of $D2^{2+}$ by means of potentiometric measurements, due to its poor solubility in the pH range above 5. However, the determination of a conditional complexation constant for the binding of Cu(II) to $D2^{2+}$ at pH 7.0 (I = 0.10 M, T = 25 °C) was achieved by means of spectrophotometric titrations (Fig. S4 of the ESI†). Such determination was necessary to evaluate the robustness of the complex under the conditions employed for DNA binding studies. Absorbance data at 283 nm were analysed by means of eqn (1)

$$\frac{C_{D2}C_{Cu}}{\Delta A} + \frac{\Delta A}{\Delta \varepsilon^2} = \frac{1}{\Delta \varepsilon}(C_{D2} + C_{Cu}) + \frac{1}{K_C \Delta \varepsilon} \quad (1)$$

where $\Delta A = A - \varepsilon_{D2}C_{D2}$, to calculate the stability constant K_c = $(1.0 \pm 0.1) \times 10^5$. This value shows that the complex is stable enough to resist demetallation in the presence of DNA, but a five-fold excess of Cu(II) is needed to ensure the quantitative transformation of the ligand into its Cu(II) complex under the conditions of the DNA binding experiments.

Protonation and complexation data for $D1^{2+}$ were reported previously.[28]

3.3. Absorption and emission spectra

The UV-vis absorption spectra of $D2^{2+}$ and $D3^{2+}$ were recorded in aqueous solution at different pH values (Fig. S5 of the ESI†). Those recorded at pH 2 and 11, corresponding, respectively, to the completely protonated and non-protonated species, are shown in Fig. 4. The spectra of $D2^{2+}$ and $D3^{2+}$ are very similar and retain most of the features of the components. They display a broad band at about 450 nm attributed to a metal-to-ligand $d\pi \rightarrow \pi^*$ charge-transfer (MLCT) independent on the nature of the ligands (bpy, dppz) coordinated to the metal, and two more bands at longer wavelengths due to ligand-centred $\pi \rightarrow \pi^*$ transitions. The broader one at about 360 nm is typical of dppz, although for free dppz this band appears as split into two almost separated peaks,[49] while the high-intensity band centred at about 280 nm is probably due to the overlap of bpy and dppz ligand-centred $\pi \rightarrow \pi^*$ transitions.[50] These spectra are consistent with those previously reported for $D1^{2+}$ and, as observed for this complex,[28] the absorption spectra of $D2^{2+}$ and $D3^{2+}$ do not change significantly with pH (Fig. 4), although some modifications (which can be related to protonation of the benzylic nitrogen atoms of the macrocyclic moiety)[28] could be detected.

In contrast with $D1^{2+}$, whose MLCT excited state is characterized by a long-lived luminescence in aqueous solution,[28] $D2^{2+}$ and $D3^{2+}$ are quenched in this solvent while they are emissive in ethanol. This is a common feature of Ru(II) complexes containing dppz or dppz derivatives which has been ascribed to proton transfer to the phenazine nitrogen atoms of the photoexcited complex.[14,15,16,17,18] Accordingly, a progressive addition of water to solutions of $D2^{2+}$ and $D3^{2+}$ in ethanol gives rise to a progressive quenching of the emission (Fig. S6 of the ESI†). This experimental evidence shows that the emission properties of these complexes are strongly influenced by the microenvironment around the dppz groups. Indeed, as thoroughly described below, interaction of $D2^{2+}$ and $D3^{2+}$ with DNA revives the MLCT excited state emission, as water molecules around dppz groups are released upon intercalation between base pairs.

3.4. DNA interaction

Equilibria. The equilibria of the ruthenium complexes binding to DNA have been investigated by both spectrophotometric and spectrofluorometric methods at pH = 7.0. The absorbance spectra for the DNA/$HD2^{3+}$ system, recorded during a spectrophotometric titration, are shown in Fig. 5a.

The spectrum displays two bands centred respectively at around 365 nm and 444 nm, the more energetic one having the features of a double band whose components tend to merge as the free-ligand is gradually converted to bound-ligand. As the titration proceeds, the main effect is an absorbance decrease (from spectrum (a) to (b)). Some absorbance increase is also observed corresponding to the highest polynucleotide loadings (from spectrum (b) to (c) of Fig. 5a). A typical binding isotherm is shown in Fig. 5b.

Concerning fluorescence, a sharp increase of emission is observed as DNA is added to the cell containing $HD2^{3+}$ (Fig. 6a); the relevant binding isotherm at λ_{em} = 610 nm is represented in Fig. 6b.

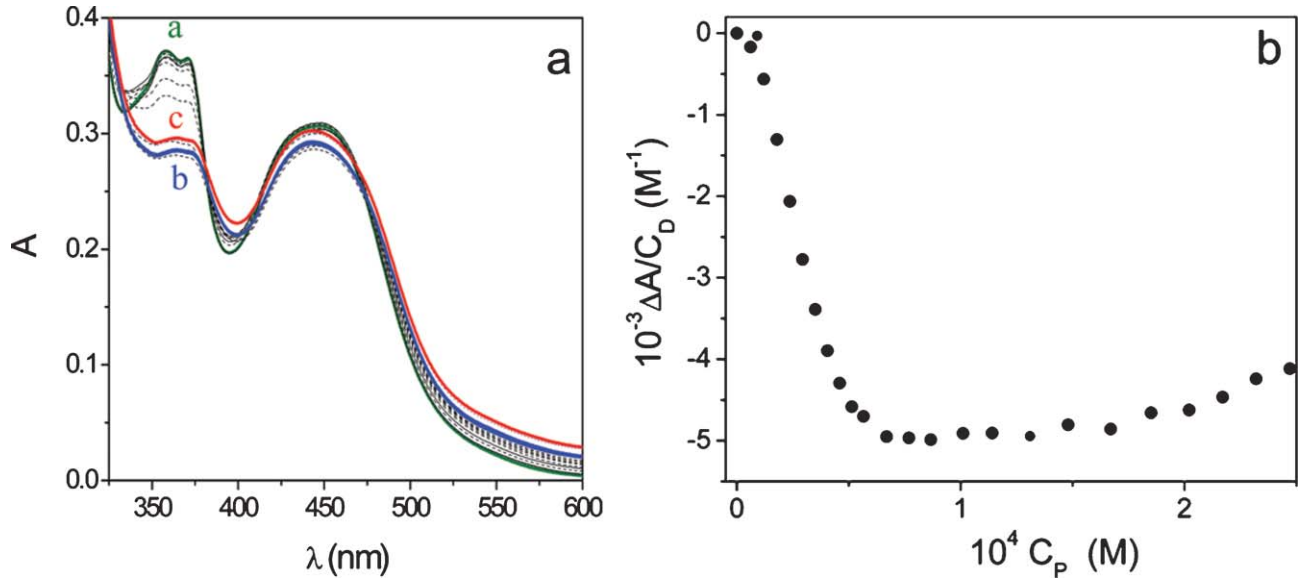

Fig. 5 Absorbance spectra for the DNA/$HD2^{3+}$ system recorded during titration (a) and relevant binding isotherm at 357 nm (b). $C_D = 2.0 \times 10^{-5}$ M, $I = 0.10$ M, pH = 7.0, $T = 25$ °C, $C_P = 0$ M (a) 7.7×10^{-5}M (b) 2.5×10^{-4}M (c).

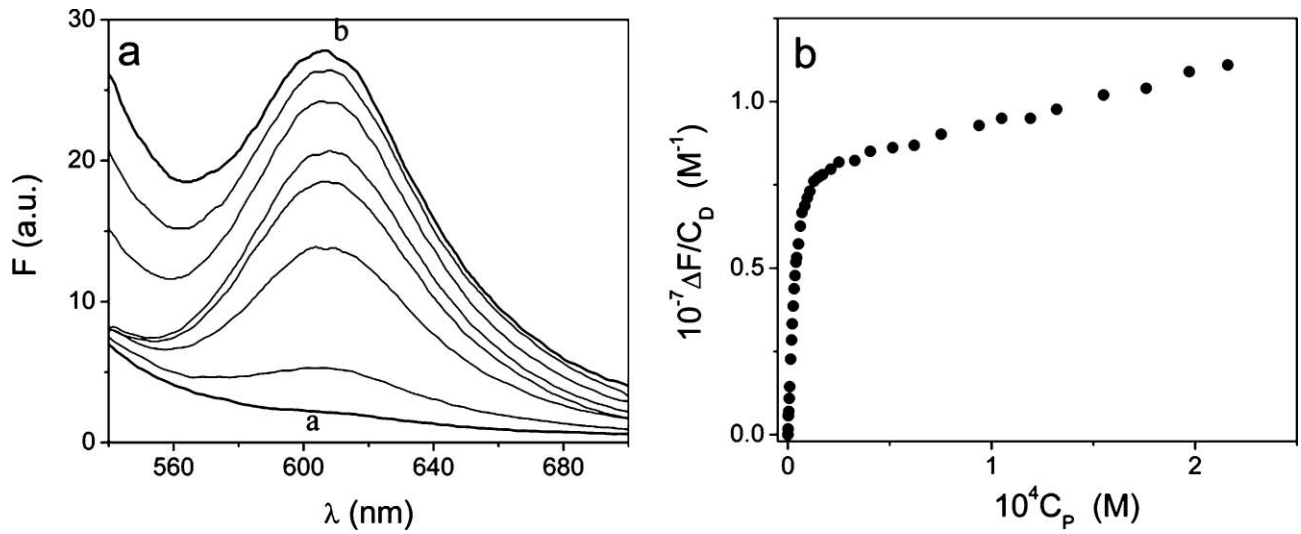

Fig. 6 Fluorescence spectra for the DNA/$HD2^{3+}$ system recorded during titration (a) and relevant binding isotherm at 610 nm (b). $C_D = 2.3 \times 10^{-6}$ M, $I = 0.10$ M, $\lambda_{ex} = 400$ nm, pH = 7.0, $T = 25$ °C, $C_P = 0$ M (a), 2.2×10^{-4} M (b).

The binding of the ruthenium complex dye, D, to a free polymer site, S, to give an occupied site DS can be expressed by the apparent reaction

$$D + S \leftrightarrows DS \tag{2}$$

Denoted as A and A_0 the optical densities of the dye in the presence of DNA lattice and in its absence respectively and as ε_i the molar extinction coefficient of the i-*th* species, it turns out that $[DS] = (A - A_0)/(\varepsilon_{DS} - \varepsilon_D) = \Delta A/\Delta\varepsilon$. Note that in fluorescence experiments ΔA and $\Delta\varepsilon$ are replaced respectively by ΔF, the difference of fluorescence signals, and $\Delta\varphi = \varphi_{DS} - \varphi_D$. The free ruthenium complex concentration [D] is equal to $C_D - [DS]$. Data can be presented according to a plot of $r/[D]$ *vs.* r where $r = [DS]/C_P$ (Fig. 7).[51] The bell-shaped trend of the plot reveals that the binding mode is cooperative.

McGhee and von Hippel derived the equation reported below, that is able to describe the cooperative binding of ligands to an homogeneous lattice.[52]

$$\frac{r}{[D]} = K \times (1 - nr) \times \left\{ \frac{(2\varpi + 1)(1 - nr) + r - R}{2(\varpi - 1)(1 - nr)} \right\}^{n-1} \times \left\{ \frac{1 - (n+1)r + R}{2(1 - nr)} \right\}^{2} \tag{3}$$

where

$$R = \sqrt{\left\{ [1 - (n+1)r]^2 + 4\varpi r(1 - nr) \right\}} \tag{4}$$

n is the number of monomer units of the polymer involved in the binding of one dye molecule under conditions of complete

Table 2 Parameters for the binding to DNA of the different ruthenium compounds analysed in the present work. pH = 7.0, T = 25 °C

	I/M	K/M^{-1}	n	ω
H_2D1^{4+}	0.10	$(1.4 \pm 0.1) \times 10^4$	1.0 ± 0.3	—
$HD2^{3+}$	0.10	$(1.4 \pm 0.2) \times 10^4$	3.1 ± 0.1	66 ± 11
$HD3^{3+}$	0.10	$(2.1 \pm 0.7) \times 10^5$	1.0 ± 0.1	—
	0.003	$(2.4 \pm 0.5) \times 10^6$	1.2 ± 0.1	—
$CuD1^{4+}$	0.10	$(3.7 \pm 0.2) \times 10^3$	1.0 ± 0.8	—
$CuD2^{4+}$	0.10	$(6.5 \pm 0.2) \times 10^4$	1.8 ± 0.1	—
$CuD3^{4+}$	0.10	$(4.8 \pm 0.9) \times 10^5$	0.8 ± 0.4	—

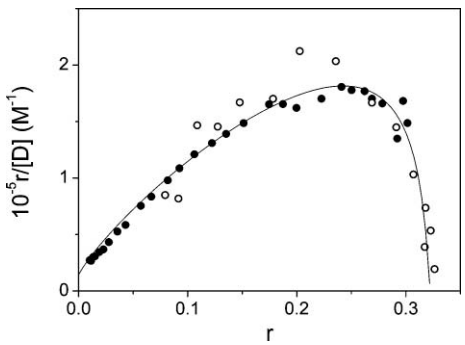

Fig. 7 McGhee and von Hippel analysis for the DNA/$HD2^{3+}$ system for both absorbance (open circles) and fluorescence (full circles) titrations data. I = 0.10 M, pH = 7.0, T = 25 °C, continuous line is data fitting to eqn (3). The drifting data at the highest DNA loadings (Fig. 5b and 6b) have been here disregarded.

saturation (site size) and ω is the cooperativity parameter. Analysis on eqn (3) of the data of Fig. 7 yields the equilibrium parameters reported in Table 2.

Similar analysis of DNA binding features (pH = 7.0) was done on the copper(II) complex of $D2^{2+}$ ($CuD2^{4+}$), $HD3^{3+}$ and its copper(II) complex ($CuD3^{4+}$), H_2D1^{4+} and its copper(II) complex ($CuD1^{4+}$).

Concerning the $CuD2^{4+}$/DNA system, as already mentioned, a five-fold copper excess is sufficient to quantitatively convert all the $D2^{2+}$ molecules into the $CuD2^{4+}$ complex ($C_{CuD24+} = C_D$). Note that, no binding of the exceeding copper ions to DNA seems to occur under these conditions.[53-56] Having established that the only species reacting with DNA is $CuD2^{4+}$, the equilibrium parameters concerning the binding of $CuD2^{4+}$ to DNA have been determined by means of the Mc Ghee and von Hippel analysis (Fig. 8). The total $CuD2^{4+}$ concentration employed in the analysis has been evaluated taking into account the stability constant of the complex ($(1.0 \pm 0.1) \times 10^5$ M^{-1}) and found to coincide with the total dye concentration (C_D) under the conditions of the experiments.

Note that now the full trend is descending; this feature indicates the absence of cooperative features in the binding process. Under these circumstances ω = 1 and experimental data can be fitted by the McGhee and von Hippel equation in the absence of cooperativity (eqn (5)).[52]

$$\frac{r}{[D]} = K \times \frac{(1-nr)^n}{[1-(n-1)r]^{n-1}} \quad (5)$$

The analysis of the data according to eqn (5) is shown as a continuous line in Fig. 8 and the reaction parameter values are collected in Table 2.

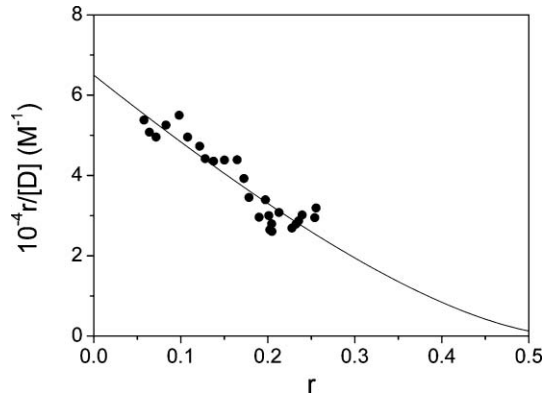

Fig. 8 McGhee and von Hippel analysis for the DNA/$CuD2^{4+}$ system, obtained by fluorescence titration data. $C_D = 9.0 \times 10^{-6}$ M, C_P from 0 to 2.2×10^{-4} M, I = 0.10 M, λ_{ex} = 400 nm, λ_{em} = 600 nm, pH = 7.0, T = 25 °C, continuous line is data fitting to eqn (5).

In order to further demonstrate the absence of cooperativity, the data were also processed according to the Schwarz theory for cooperative binding.[57] The equilibrium constant K of the growth step can be determined together with the cooperativity parameter ω from best fits to eqn (6)

$$(1 - 2\theta)([D]/(\theta(1-\theta))^{1/2} = (\omega/K)^{1/2} - (\omega K)^{1/2}\,[D] \quad (6)$$

where θ is the fraction of occupied sites $\theta = n[DS]/C_P = nr$, with n = 1.8. The fit shown in Fig. S7 of the ESI† yields $\omega \approx 1$, confirming that the binding mode operative in the DNA/$CuD2^{4+}$ system does not display cooperative features. It also turns out that $K = (8.5 \pm 0.4) \times 10^4$ M^{-1}, is in good agreement with the evaluation made according to eqn (5).

The behaviour of the DNA/$HD3^{3+}$ and DNA/$CuD3^{4+}$ systems is similar to that of the DNA/$CuD2^{4+}$ system and no cooperativity is observed. In the case of the DNA/$CuD3^{4+}$ system, owing to the much higher stability constant of the $CuD3^{4+}$complex (Table 1), equimolar addition of Cu^{2+} ions is sufficient to ensure quantitative formation of $CuD3^{4+}$ under the conditions of complex binding to DNA. Fluorescence titrations are analysed for both DNA/$HD3^{3+}$ and DNA/$CuD3^{4+}$ systems using eqn (5) (see Fig. S8 and S9 of the ESI†) and the values of the binding parameters obtained are collected in Table 2. As previous studies on the $Ru(phen)_2dppz^{2+}$ complex pointed out the importance of low added salt content measurements to reveal the occurrence of an additional binding mode,[20] absorbance titrations were repeated for the DNA/$HD2^{3+}$ and DNA/$HD3^{3+}$ systems at I = 0.003 M (pH = 7.0) (Fig. S10 of the ESI†). As regards the DNA/$HD3^{3+}$ system, no significant variation in the shape of the binding isotherm is observed; the binding curve is analysed by means of eqn (5) and the results are given in Table 2. On the contrary, significant changes occur under the above experimental conditions in the case of DNA/$HD2^{3+}$; actually the slight absorbance increase observed at I = 0.1 M (Fig. 5) now turns into a steep rise in the signal that reaches a plateau. Application of eqn (5) on this part of the plot yields $K = (1.1 \pm 0.1) \times 10^4$ M^{-1} and $n = 0.7 \pm 0.4$. At the end of the titration (high DNA excess), precipitation phenomena are observed. On the other hand, the initial descending part of the plot is connected to a remarkably high constant whose lower limit only can be estimated ($K > 10^7$ M^{-1}).

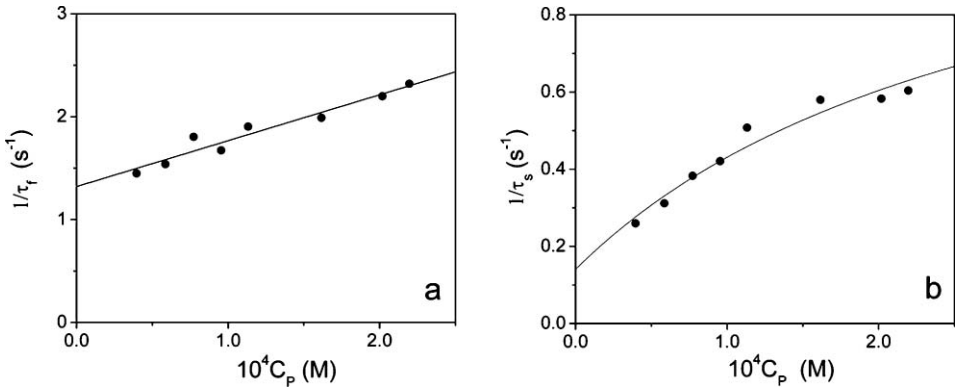

Fig. 9 Dependence of the reciprocal (a) fast ($1/\tau_f$) and (b) slow ($1/\tau_s$) relaxation times on the excess reagent concentration (C_P) for the DNA/HD2^{3+} system. $I = 0.1$ M, pH = 7.0, $\lambda = 360$ nm, $T = 25$ °C; continuous lines are data fitting to eqn (8) and (9) respectively.

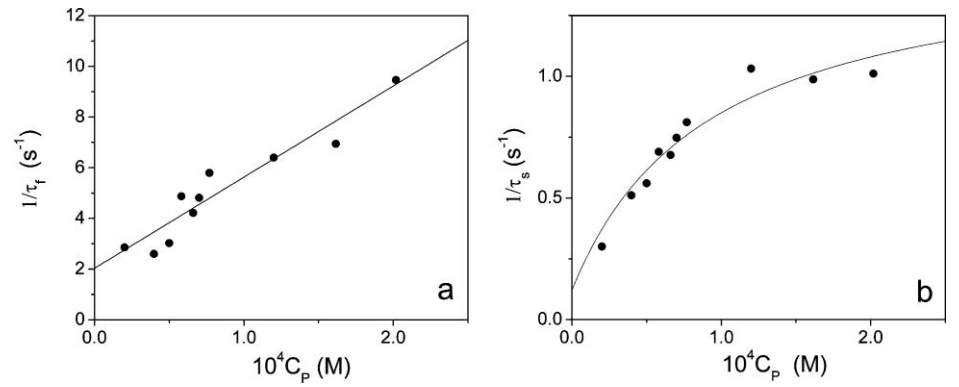

Fig. 10 Dependence of the reciprocal (a) fast ($1/\tau_f$) and (b) slow ($1/\tau_s$) relaxation times on the excess reagent concentration (C_P) for the DNA/HD3^{3+} system. $I = 0.1$ M, pH = 7.0, $\lambda = 360$ nm, $T = 25$ °C; continuous lines are data fitting to eqn (8) and (9) respectively.

Experiments on the DNA/H_2D1^{4+} system were also carried out for comparison purposes. Absorbance titrations (Fig. S11 of the ESI†) did not reveal any variation in the visible part of the dye spectrum upon DNA addition; on the other hand, in the UV range, dye absorbance decrease indicates some DNA/dye interaction is also occurring in the case of the H_2D1^{4+} complex. The relevant binding isotherm (inset of Fig. S9C†) shows a first binding process with a remarkably high constant whose lower limit only can be estimated ($K > 10^6$ M^{-1}), followed by a decrease of absorbance. Fluorescence titrations (Fig. S12 of the ESI†) provide a better estimation of the binding process. The biphasic binding isotherm reveals the presence of a first binding mode (dye excess conditions), related to fluorescence decrease ($K > 3 \times 10^6$ M^{-1}) followed by a non cooperative mode of binding whose parameters, calculated by means of eqn (5), are collected in Table 2. Spectrofluorometric titrations of the DNA/CuD1^{4+} system yielded results similar to those shown for DNA/H_2D1^{4+} (Fig. S13 of the ESI†). The binding parameters for the main binding mode (fluorescence increase under polymer excess conditions) are given in Table 2; as regards the additional binding observed under dye excess conditions the analysis by means of eqn (5) yields $K = (2.1 \pm 0.5) \times 10^4$ M^{-1}.

To test the eventual cleavage ability of the here analysed metal-intercalators, electrophoresis experiments were carried out on the DNA/HD2^{3+}, DNA/CuD2^{4+}, DNA/HD3^{3+} and DNA/CuD3^{4+} systems, alone or in the presence of H_2O_2. The results are shown in Fig. S14 of the ESI.† The higher band mobility of the CuD3^{4+} complex, suggesting polynucleotide cleavage, is observed only in the presence of H_2O_2. So CuD3^{4+} is the species that seems to produce polynucleotide alterations.

Kinetics. The kinetic study of HD2^{3+} and HD3^{3+} binding to DNA was performed by the stopped-flow technique under DNA excess. Under these circumstances, the binding of the complex to DNA occurs at isolated sites. For both DNA/HD2^{3+} and DNA/HD3^{3+} systems the kinetic curves display a bi-exponential behaviour (Fig. S15 of the ESI†). The analysis of the kinetic data is made, for each system, by plotting the reciprocal of the two relaxation times, $1/\tau_f$ and $1/\tau_s$, on the concentration of the excess reagent, C_P (Fig. 9 and 10).

Considering the two-step series mechanism

$$P + D \underset{k_{-1}}{\overset{k_1}{\rightleftharpoons}} PD_I \underset{k_{-2}}{\overset{k_2}{\rightleftharpoons}} PD_{II} \quad (7)$$

where P and D are a free DNA site and free dye respectively, whereas PD_I and PD_{II} are conformationally different complexes, data have been fitted to eqn (8) and (9).

$$\frac{1}{\tau_f} = k_1 C_P + k_{-1} \quad (8)$$

$$\frac{1}{\tau_s} = \frac{K_1 k_2 C_P}{1 + K_1 C_P} + k_{-2} \quad (9)$$

Table 3 Kinetic parameters for $HD2^{3+}$ and $HD3^{3+}$ binding to DNA. $I = 0.10$ M, pH = 7.0, $T = 25$ °C. For the meaning of the parameters refer to scheme (7)

	$10^{-5}K/M^{-1}$	[a] $10^{-3}K_1/M^{-1}$	[b] K_2	$10^{-3}k_1/M^{-1}s^{-1}$	k_{-1}/s^{-1}	k_2/s^{-1}	k_{-2}/s^{-1}
$HD2^{3+}$	[c] 0.30 ± 0.12	3.4 ± 0.5	8 ± 2	4.5 ± 0.5	1.3 ± 0.1	1.1 ± 0.1	0.14 ± 0.03
$HD3^{3+}$	[d] 2.1 ± 0.7	18 ± 6	11 ± 7	36 ± 4	2.0 ± 0.4	1.4 ± 0.1	0.13 ± 0.09

[a] $K_1 = k_1/k_{-1}$; [b] $K_2 = k_2/k_{-2}$; [c] from kinetics $K = K_1(1+K_2)$; [d] from static measurements – Table 2.

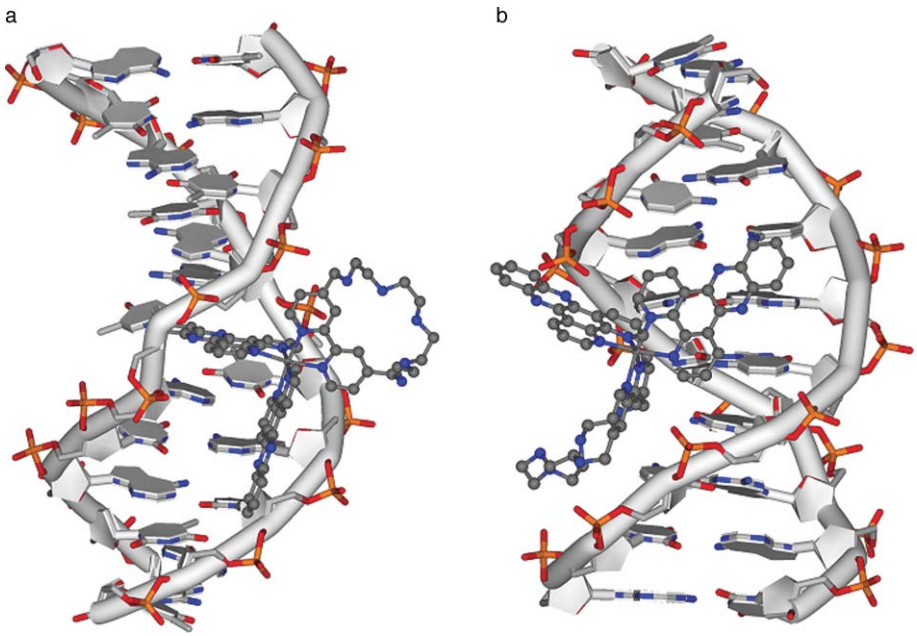

Fig. 11 Calculated models for intercalative (a) and groove (b) binding in $HD3^{2+}$/DNA adducts.

where $K_1 = k_1/k_{-1}$. Note that for the DNA/$HD3^{3+}$ system the value of k_{-2} can only with very low accuracy be determined from data fit to eqn (9). On the other hand, a better k_{-2} estimation can be obtained owing to the relationship $K = K_1(1 + K_2) = K_1(1 + k_2/k_{-2})$, where K, the overall binding constant, is known from the static measurements. The values of the obtained reaction parameters of the different steps of scheme 7 are collected in Table 3.

Molecular modelling. Docking calculations carried out for $HD2^{3+}$, H_2D2^{4+}, $HD3^{3+}$ and H_2D3^{4+} and five B-DNA decamers evidenced that the two complexes are able to interact with double stranded DNA in both Λ and Δ configurations *via* intercalative and groove binding processes. Also in this section we will refer to these complexes as $HD2^{3+}$ and $HD3^{3+}$, since no significantly different behaviours were observed for the differently protonated species. Images of the poses obtained for the DNA adducts are shown in Fig. 11 and 12 and Fig. S16–S27 of the ESI,† the former (Fig. 11 and 12) being representative of all the binding modes found for these Ru(II) complexes.

The two complexes, however, display rather different behaviours. Actually, for all the investigated sequences, fewer poses were obtained for the bulkier $HD3^{3+}$ complex with respect to $HD2^{3+}$ (Fig. S16–S27 of the ESI†). In addition, in the case of $HD2^{3+}$ (Fig. S21–S27 of the ESI†), the intercalative binding clearly prevails on the groove one and the polyamine chain of the macrocyclic moiety gives rise more easily to H-bond or salt bridge contacts with DNA than $HD3^{3+}$. Results of docking procedures carried out in order to investigate the possible occurrence of dye–dye interactions, which might explain the cooperative behaviour observed for $HD2^{3+}$, are shown in Fig. 12b. The analysis of the binding mode of the second $HD2^{3+}$ molecule shows both external interaction with the double stranded DNA *via* H-bonding involving a DNA phosphate group and a complex aliphatic nitrogen atom, and CH···π dye–dye interaction, involving the bipyridine groups of the external and the intercalated $HD2^{3+}$ molecules. Most likely, further interaction occurs between the bipyridine group of the intercalated $HD2^{3+}$ molecule and the dppz moiety of the external $HD2^{3+}$. Conversely, in the case of $HD3^{3+}$, no poses were found in which $HD3^{3+}$ gives rise to simultaneous dye–dye and dye–DNA interactions.

4. Discussion

The previously determined crystal structure of $(H_3D1)(ClO_4)_5 \cdot H_2O$ showed the Ru(II) cation surrounded by an octahedral coordination environment defined by three bipyridine groups, one of which supports the cyclic penta-aza aliphatic chain bearing the three acidic H^+ ions.[28] This protonated ring protrudes from the complex core assuming a fairly flat conformation to interact *via* electrostatic attraction and hydrogen bonding with ClO_4^- counterions. Accordingly, the protonated polyamine chain is expected to also be able to interact with the phosphate backbone of DNA. Taking into account the thermodynamic and kinetic

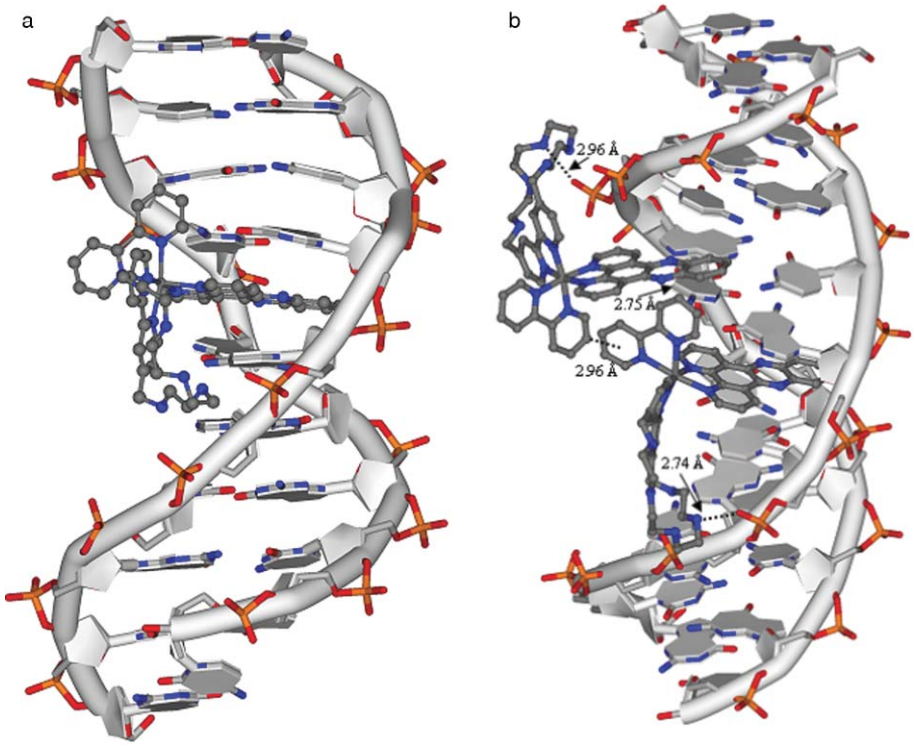

Fig. 12 Calculated model for intercalative binding in the $HD2^{3+}$/DNA adduct (a) and dye–dye interaction responsible for cooperative behaviour in the binding of $HD2^{3+}$ to double stranded DNA (b).

robustness of the central metal ions and the planar, rigid structure of dppz, the structures of $D2^{2+}$ and $D3^{2+}$ complexes can be reasonably thought as deriving from the mere substitution of bipyridine groups with dppz. Hence, the three dyes offer a range of different binding possibilities toward DNA, coupling the electrostatic attraction and hydrogen bonding ability of the protonated polyamine chain with the intercalating and/or groove binding properties of bipyridine and dppz molecules. Binding of Cu(II) at the polyamine chain gives rise to further possibilities for interaction with DNA. As observed above, Cu(II) is expected to be coordinated to no more than four nitrogen atoms of the ligand L attached to the Ru(II) complexes, further coordinative positions being available for interaction with exogenous species. As a matter of fact, the crystal structure of the $Cd_3L_2Br_6$ complex showed that the ligand L, attached to a metal ion through the external bipyridine group, binds a second Cd(II) ion within the macrocyclic ring by using only four aliphatic amine groups, leaving open access to penetration of two Br^- anions into the coordination sphere of this metal ion.

Accordingly, the present study shows that the synthesised complexes do interact with DNA, but the binding mode is not simple and its features strongly depend both on the ligand nature and on the C_P/C_D ratio, since lateral effects are observed under conditions of dye or polymer excess. Previous studies on DNA binding by similar ruthenium complexes[19,20,58,59] have shown that intercalation or external binding can both be operative. For the $D2^{2+}$ and $D3^{2+}$ complexes, the major binding mode (Table 2), associated to a sharp increase of fluorescence emission and some red shift of the absorption spectra maximum around 365 nm, is consistent with the intercalative stacking of the dppz residue between base pairs already observed for similar ruthenium and osmium complexes.[7,60-62] However, in the case of the DNA/$HD2^{3+}$ system, an important contribution of external interactions has to be considered, as suggested by the positive cooperativity exhibited by the system. Dye–dye interaction is considered to be a cause for cooperative behaviour[57,63] and could likely be operating in the binding of $HD2^{3+}$ to DNA, leading to geometries such that the site size (n) increases (Table 2). Indeed, modelling calculations clearly show that interaction between the intercalated $HD2^{3+}$ complex and a second complex molecule externally bound occurs, mostly due to a CH $\cdots$ π contact between their bipyridine groups. On the contrary, for the bulkier $HD3^{3+}$ complex, dye–dye interactions seem to be less effective, leading to an intercalating process where higher freedom of dyes positioning yields lower n values. According to the modelling results, showing that no simultaneous dye–dye and dye–DNA interactions occur in the case of $HD3^{3+}$, the bulkier dppz moiety present in $HD3^{3+}$ as compared to the bipyridine in $HD2^{3+}$, most likely hinders the entrance of the second $HD3^{3+}$ molecule in close proximity, once the first one has already interacted with the double stranded DNA. Blank experiments on DNA/H_2D1^{4+} enlighten the contribution of the azamacrocycle to the overall binding. The affinity for DNA of the $Ru(bpy)_3^{2+}$ complex being very low (10^2 M^{-1} at I = 0.05 M, pH 7.5 and 20 °C),[64,65] the remarkably higher K value found in the present study for H_2D1^{4+} has to be related to the interaction of the positively charged poly-amino ring with the negatively charged polynucleotide backbone. The binding affinity of the $CuD1^{4+}$ complex is significantly lower than that of H_2D1^{4+}; whereas for $HD2^{3+}$ and $HD3^{3+}$ copper complexation results in a slight increase of K (Table 2), in agreement with the higher positive charge

borne by the complexes.[66] These results suggest that the ring rigidity increase, caused by metal ion complexation, significantly contributes to reduction of the binding affinity only in the case of the $D1^{2+}$ complex. In the case of $D2^{2+}$, copper complexation causes in the DNA/$CuD2^{4+}$ system the loss of the cooperative features observed for DNA/$HD2^{3+}$. As regards the potential of the copper complexes to produce the cleavage of DNA it can also be noted that the $CuD2^{4+}$ complex seems to lose the cleavage ability displayed by copper ions, which is on the contrary retained by $CuD3^{4+}$. This finding could be indicative of a positioning of the coordinated metal ion much further from the phosphate backbone in the case of the $D2^{2+}$ complex (Fig. 12b).

A binding mode, occurring under polymer excess conditions and strongly influenced by the medium ionic strength, was observed for the DNA/$Ru(phen)_2dppz^{2+}$ system,[20] and ascribed to partial dppz residue intercalation whereas phenanthroline residue allocates in the groove. In the present study, absorbance and fluorescence signal deviations from the expected plateau under DNA excess conditions could suggest some similar external binding is possible (although with low affinity). This dual behaviour cannot be likely ascribed to the Δ and Λ isomers, as it was found that the thermodynamics of the binding do not significantly depend on the complex chirality.[19,20,67] The additional binding mode observed at high complex loadings only in the case of H_2D1^{4+} can likely be ascribed to the (crowded) dye accommodation into the polynucleotide grooves, since its dimensions[23] are consistent with those of the B-DNA groove.[68]

The static experiments show that the binding affinity for DNA is higher for $D3^{2+}$ (two dppz residues) with respect to $D2^{2+}$ (one dppz residue) and this difference in the binding features is confirmed by the kinetic experiments (Table 3). The two-step binding mechanism (scheme 7) can be interpreted in terms of conversion from an initial external (or partially intercalated) state (PD_I formation) to a final intercalated state (PD_{II}).[69] It can be noted that the higher value of the overall binding constant for $HD3^{3+}$ with respect to $HD2^{3+}$ corresponds to a higher K_1 value. As the k_{-1} parameters are similar for the two systems, this result should be ascribed to the k_1 value that is significantly higher for $HD3^{3+}$ with respect to $HD2^{3+}$. This finding is in agreement with the model where the intercalation of the bulkier $HD3^{3+}$ complex occurs with less energy penalty with respect to $HD2^{3+}$, to yield a form that shows a reduced degree of ligand penetration. Partial intercalation of $HD3^{3+}$ is confirmed by the obtained values of the site size, which are close to unity. The differences observed for the first binding step are not observed in the second one, all parameters related to step II being very similar for the two systems. This finding could be interpreted assuming that the common macrocyclic structure is involved in the second step.

It should be noted that the values of k_1 are lower by at least four orders of magnitude with respect to a bimolecular diffusion controlled encounter, thus indicating that the first step of scheme (7) is not an elementary one. Therefore, scheme (7) can be expanded according to the sequence (10)

$$P + D \underset{}{\overset{K_0}{\rightleftharpoons}} P,D \underset{k_{-1}}{\overset{k'_1}{\rightleftharpoons}} PD_I \underset{k_{-2}}{\overset{k_2}{\rightleftharpoons}} PD_{II} \qquad (10)$$

where K_0 is the equilibrium constant of a diffusion controlled step leading to formation of a precursor complex, P,D. By comparing schemes (7) and (10) it turns out that $k_1 = K_0\, k_1'/(1 + K_0([P]+[D]))$.

The linear fits of $1/\tau_f$ *vs.* [P]+[D] plots (Fig. 9A and 10A) reveal that for both the analysed systems K_0 ([P]+[D])$\ll$1. This feature only enables the product $K_0\, k_1'$ to be obtained, which corresponds to k_1 of scheme (6). On the other hand, it should be noted that, in order to produce significant deviations from the linear trends, K_0 values higher than 2000 M^{-1} are required. The upper limit for K_0 can thus be obtained. The constant for an electrostatic binding between a +3 charged dye and a DNA base pair, calculated correcting for charge effects the value of Mayer–Almes and Pörscke related to a +1 dye[70] with the help of the Fuoss equation,[66] turns out to be *ca.* 1000 M^{-1}. On this basis, it can be supposed that stabilization of the precursor complex P,D is essentially provided by electrostatic forces, which should be similar because $HD2^{3+}$ and $HD3^{3+}$ bear the same charge. This finding enables us to assert that any difference of the reaction parameters emerging from comparison of the data of Table 3 should be ascribed to the different structures of the two complexes.

References

1 K. E. Augustyn, V. C. Pierre and J. K. Barton, in *Wiley Encyclopedia of Chemical Biology*, ed. T. P. Begley, J. Wiley and Sons Inc., 2009, vol. 3, pp. 34–45.
2 A. M. Pyle and J. K. Barton, in *Progress in Inorganic Chemistry: Bioinorganic Chemistry*, ed. J. Stephen Lippard, J. Wiley and Sons Inc., 1990, vol. 38, pp. 413–475.
3 C. Moucheron, *New J. Chem.*, 2009, **33**, 235–245.
4 I. Kostova, *Curr. Med. Chem.*, 2006, **13**, 1085–1107.
5 F. Gonzalez-Vilchez, R. Vilaplana, in *Metal Compounds in cancer chemotherapy*, ed. J. M. Perez, M. A. Fuertes and C. Alonso, 2005, pp. 321–354.
6 F. Gao, H. Chao and L.-N. Ji, *Chem. Biodiversity*, 2008, **5**, 1962–1979.
7 A. E. Friedman, J.-C. Chambron, J.-P. Sauvage, N. J. Turro and J. K. Burton, *J. Am. Chem. Soc.*, 1990, **112**, 4960–4962.
8 K. E. Erkkila, D. T. Odom and J. K. Barton, *Chem. Rev.*, 1999, **99**, 2777–2795.
9 M. Navarro, E. J. Cisneros-Fajardo, A. Sierralta, M. Fernandez-Mestre, P. Silva, D. Arrieche and E. Marchan, *J. Biol. Inorg. Chem.*, 2003, **8**, 401–408.
10 F. Westlund, F. Pierard, M. P. Eng, B. Nordén and P. Lincoln, *J. Phys. Chem. B*, 2005, **109**, 17327–17332.
11 W. R. Browne and J. J. McGarvey, *Coord. Chem. Rev.*, 2006, **250**, 1696–1709.
12 Q. G. Mulazzani, M. D'Angelantonio, M. Venturi, M. L. Boillot, J. C. Chambron and E. Amouyal, *New J. Chem.*, 1989, **13**, 441–447.
13 J.-C. Chambron and J.-P. Sauvage, *Chem. Phys. Lett.*, 1991, **182**, 603–607.
14 E. Amouyal, A. Homsi, J.-C. Chambron and J.-P. Sauvage, *J. Chem. Soc., Dalton Trans.*, 1990, 1841–1845.
15 B. Gholamkhass, K. Koike, N. Negishi, H. Hori and K. Takeuchi, *Inorg. Chem.*, 2001, **40**, 756–765.
16 R. B. Nair, B. M. Cullum and C. J. Murphy, *Inorg. Chem.*, 1997, **36**, 962–965.
17 C. Turro, S. H. Bossmann, Y. Jenkins, J. K. Barton and N. J. Turro, *J. Am. Chem. Soc.*, 1995, **117**, 9026–9032.
18 R. E. Holmlin, J. A. Yao and J. K. Barton, *Inorg. Chem.*, 1999, **38**, 174–189.
19 I. Haq, P. Lincoln, D. Suh, B. Nordén, B. Z. Chowdhry and J. B. Chaires, *J. Am. Chem. Soc.*, 1995, **117**, 4788–4796.
20 T. Biver, C. Cavazza, F. Secco and M. Venturini, *J. Inorg. Biochem.*, 2007, **101**, 461–469.
21 T. Biver, F. Secco, M. R. Tinè, M. Venturini, A. Bencini, A. Bianchi and C. Giorgi, *J. Inorg. Biochem.*, 2004, **98**, 1531–1538.
22 T. Biver, D. Lombardi, F. Secco, M. R. Tinè, M. Venturini, A. Bencini, A. Bianchi and B. Valtancoli, *Dalton Trans.*, 2006, 1524–1533.
23 C. Lodeiro, A. J. Parola, F. Pina, C. Bazzicalupi, A. Bencini, A. Bianchi, C. Giorgi, A. Masotti and B. Valtancoli, *Inorg. Chem.*, 2001, **40**, 2968–2975.

24 C. Anda, C. Bazzicalupi, A. Bencini, A. Bianchi, P. Fornasari, C. Giorgi, B. Valtancoli, C. Lodeiro, A. J. Parola and F. Pina, *Dalton Trans.*, 2003, 1299–1307.
25 P. Arranz, C. Bazzicalupi, A. Bencini, A. Bianchi, S. Ciattini, P. Fornasari, C. Giorni and B. Valtancoli, *Inorg. Chem.*, 2001, **40**, 6383–6389.
26 A. Bencini, A. Bianchi, S. Del Piero, C. Giorgi, A. Melchior, R. Portauova, M. Tolazzi and B. Valtancoli, *J. Solution Chem.*, 2008, **37**, 503–517.
27 C. Bazzicalupi, A. Bencini, A. Bianchi, A. Danesi, E. Faggi, C. Giorgi, C. Lodeiro, E. Oliveira, F. Pina and B. Valtancoli, *Inorg. Chim. Acta*, 2008, **361**, 3410–3419.
28 C. Lodeiro, F. Pina, A. J. Parola, A. Bencini, A. Bianchi, C. Bazzicalupi, S. Ciattini, C. Giorgi, A. Masotti, B. Valtancoli and J. Seixas de Melo, *Inorg. Chem.*, 2001, **40**, 6813–6819.
29 J. E. Dickeson and L. A. Summers, *Aust. J. Chem.*, 1970, **23**, 1023–1027.
30 P. A. Anderson, G. B. Deacon, K. H. Haarmann, F. R. Keene, T. J. Meyer, D. A. Reitsma, B. W. Skelton, G. F. Strouse, N. C. Thomas, J. A. Treadway and A. H. White, *Inorg. Chem.*, 1995, **34**, 6145–6157.
31 A. Bianchi, L. Bologni, P. Dapporto, M. Micheloni and P. Paoletti, *Inorg. Chem.*, 1984, **23**, 1201–1205.
32 G. Gran, *Analyst*, 1952, **77**, 661–671.
33 P. Gans, A. Sabatini and A. Vacca, *Talanta*, 1996, **43**, 1739–1753.
34 A. K. Covington, M. Paabo, R. A. Robinson and R. G. Bates, *Anal. Chem.*, 1968, **40**, 700–706.
35 Maestro v7.5, Schrödinger L. L. C. New York (http://www.schrodinger.com).
36 R. Andres, M. Gruselle, B. Malezieux, M. Verdaguer and J. Vaissermann, *Inorg. Chem.*, 1999, **38**, 4637–4646.
37 Jaguar, v 6.5; Schrödinger L. L. C. New York (http://www.schrodinger.com).
38 A. D. Becke, *J. Chem. Phys.*, 1993, **98**, 1372–1380; A. D. Becke, *J. Chem. Phys.*, 1993, **98**, 5648–5657; B. Miehlich, A. Savin, H. Stoll and H. Preuss, *Chem. Phys. Lett.*, 1989, **157**, 200–208.
39 P. J. Hay and W. R. Wadt, *J. Chem. Phys.*, 1985, **82**, 299–308.
40 R. A. Friesner, J. L. Banks, R. B. Murphy, T. A. Halgren, J. Klicic, D. T. Mainz, M. P. Repasky, E. H. Knoll, M. Shelley, J. K. Perry, D. E. Shaw, P. Francis and P. S. Shenkin, *J. Med. Chem.*, 2004, **47**, 1739–1749; L. L. C. Schrödinger, New York (http://www.schrodinger.com).
41 J. L. Banks, H. S. Beard, Y. X. Cao, A. E. Cho, W. Damm, R. Farid, A. K. Felts, T. A. Halgren, D. T. Mainz, J. R. Maple, R. Murphy, D. M. Philipp, M. P. Repasky, L. Y. Zhang, B. J. Berne, R. A. Friesner, E. Gallicchio and R. M. Levy, *J. Comput. Chem.*, 2005, **26**, 1752–1780.
42 Qsite, Schrödinger L. L. C., New York (http://www.schrodinger.com).
43 M. C. Cortis and R. A. Friesner, *J. Comput. Chem.*, 1997, **18**, 1591–1608.
44 P. A. Lay, A. M. Sargeson and H. Taube, *Inorg. Synth.*, 1986, **24**, 291–299; B. P. Sullivan, D. J. Salmon and T. J. Meyer, *Inorg. Chem.*, 1978, **17**, 3334–3341.
45 P. A. Anderson, G. B. Deacon, K. H. Haarmann, F. R. Keene, T. J. Meyer, D. A. Reitsma, B. W. Skelton, G. F. Strouse, N. C. Thomas, J. A. Treadway and A. H. White, *Inorg. Chem.*, 1995, **34**, 6145–6157.
46 N. Nickita, M. J. Belousoff, A. I. Bhatt, A. M. Bond, G. B. Deacon, G. Gasser and L. Spiccia, *Inorg. Chem.*, 2007, **46**, 8638–8651.
47 G. B. Deacon, C. M. Kepter, N. Sahely, B. W. Skelton, L. Spiccia, N. C. Thomas and A. H. White, *J. Chem. Soc., Dalton Trans.*, 1999, 275–277.
48 A. Bencini, A. Bianchi, E. Garcia-España, M. Micheloni and J. A. Ramirez, *Coord. Chem. Rev.*, 1999, **188**, 97–156.
49 M. Yamada, Y. Tanaka and Y. Yoshimoto, *Bull. Chem. Soc. Jpn.*, 1992, **65**, 1006–1011.
50 C.-S. Choi, L. Mishra, T. Mutai and K. Araki, *Bull. Chem. Soc. Jpn.*, 2000, **73**, 2051–2058.
51 G. Scatchard, *Ann. N. Y. Acad. Sci.*, 1949, **51**, 660–672.
52 J. D. McGhee and P. H. von Hippel, *J. Mol. Biol.*, 1974, **86**, 469–489.
53 G. L. Eichorn and P. Clark, *Proc. Natl. Acad. Sci. U. S. A.*, 1965, **53**, 586–593.
54 G. L. Eichorn, P. Clark and E. D. Becker, *Biochemistry*, 1966, **5**, 245–253.
55 A. M. Fiskin and M. Beer, *Biochemistry*, 1965, **4**, 1289–1294.
56 J. Eisinger, R. G. Shulman and B. M. Szymanski, *J. Chem. Phys.*, 1962, **36**, 1721–1729.
57 G. Schwarz, *Eur. J. Biochem.*, 1970, **12**, 442–453.
58 R. E. Holmlin and J. K. Barton, *Inorg. Chem.*, 1995, **34**, 7–8.
59 D. Z. M. Coggan, I. S. Haworth, P. J. Bates, A. Robinson and A. Rodger, *Inorg. Chem.*, 1999, **38**, 4486–4497.
60 R. E. Holmlin, E. D. A. Stemp and J. K. Barton, *J. Am. Chem. Soc.*, 1996, **118**, 5236–5244.
61 C. Hiort, P. Lincoln and B. Nordén, *J. Am. Chem. Soc.*, 1993, **115**, 3448–3454.
62 C. M. Dupureur and J. K. Barton, *J. Am. Chem. Soc.*, 1994, **116**, 10286–10287.
63 T. Biver, C. Ciatto, F. Secco and M. Venturini, *Arch. Biochem. Biophys.*, 2006, **452**, 93–101.
64 A. M. Pyle, J. P. Rehmann, R. Meshoyrer, C. V. Kumar, N. J. Turro and J. K. Barton, *J. Am. Chem. Soc.*, 1989, **111**, 3051–3058.
65 P. Lincoln and B. Nordén, *J. Phys. Chem. B*, 1998, **102**, 9583–9594.
66 R. M. Fuoss, *J. Am. Chem. Soc.*, 1958, **80**, 5059–5061.
67 P. P. Pellegrini and J. R. Aldrich-Wright, *Dalton Trans.*, 2003, 176–183.
68 U. Heinemann, C. Alings and M. Bansal, *EMBO J.*, 1992, **11**, 1931–1939.
69 F. Westerlund, L. M. Wilhelmsson, B. Nordén and P. Lincoln, *J. Phys. Chem. B*, 2005, **109**, 21140–21144.
70 F. J. Meyer-Almes and D. Pörschke, *Biochemistry*, 1993, **32**, 4246–4253.

